THE JOURNAL OF PHYSICAL CHEMISTRY Letters

Letter

Cite This: J. Phys. Chem. Lett. 2019, 10, 4374−4381

pubs.acs.org/JPCL

Electronic Preresonance Stimulated Raman Scattering Imaging of Red-Shifted Proteorhodopsins: Toward Quantitation of the Membrane Potential

Hyeon Jeong Lee,[†,‡,§] Kai-Chih Huang,[‡,§] Gaoxiang Mei,[§,#] Cheng Zong,[†,§] Natalia Mamaeva,[§,#] Willem J. DeGrip,[∥,¶] Kenneth J. Rothschild,[*,§,#,⊥] and Ji-Xin Cheng[*,†,‡,§,#]

[†]Department of Electrical and Computer Engineering, Boston University, Boston, Massachusetts 02215, United States

[‡]Department of Biomedical Engineering, Boston University, Boston, Massachusetts 02215, United States

[§]Photonics Center, Boston University, Boston, Massachusetts 02215, United States

[#]Department of Physics, Boston University, Boston, Massachusetts 02215, United States

[∥]Department of Biophysical Organic Chemistry, Leiden Institute of Chemistry, Leiden University, 2300 RA Leiden, The Netherlands

[¶]Department of Biochemistry, Radboud University Medical School, 6500 HB Nijmegen, The Netherlands

[⊥]Department of Physiology and Biophysics, Boston University School of Medicine, Boston, Massachusetts 02218, United States

Supporting Information

ABSTRACT: Voltage imaging allows mapping of the membrane potential in living cells. Yet, current intensity-based imaging approaches are limited to relative membrane potential changes, missing important information conveyed by the absolute value of the membrane voltage. This challenge arises from various factors affecting the signal intensity, such as concentration, illumination intensity, and photobleaching. Here, we demonstrate electronic preresonance hyperspectral stimulated Raman scattering (EPR-hSRS) for spectroscopic detection of the membrane voltage using a near-infrared-absorbing microbial rhodopsin expressed in *E. coli*. This newly developed near-infrared active microbial rhodopsin enables electronic preresonance SRS imaging at high sensitivity. By spectral profiling, we identified voltage-sensitive SRS peaks in the fingerprint region in single *E. coli* cells. These spectral signatures offer a new approach for quantitation of the absolute membrane voltage in living cells.

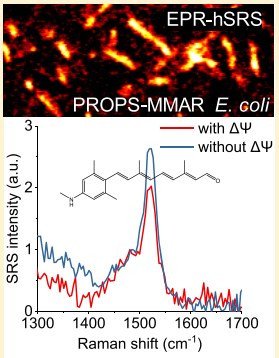

The development of imaging techniques to monitor and map action potentials in complex neural circuits has enabled neuroscientists to gain new understanding of brain function[1,2] and holds great promise for diagnosing and treating brain disorders.[3] The most widely adopted approach is via fluorescence imaging of voltage-sensitive dyes or proteins, in which the fluorescent intensity monitors the change of membrane potentials.[2] Genetically encoded voltage reporters (e.g., optogenetic reporters) are especially advantageous due to their ability to label specific subtypes of neurons.[2] Significant progress has also been made in developing voltage reporters with improved signal-to-noise ratio (SNR), voltage sensitivity, membrane localization, voltage response speed, stability of fluorescence, and red-shifted spectral profiles by using directed molecular evolution.[2,4,5] Among these properties, the ability to absorb near-infrared (NIR) light is gaining attention because NIR light can penetrate deeper into biological tissues due to reduced scattering and absorption.[6] However, it is challenging to generate NIR-absorbing proteins while retaining other desired properties such as voltage sensitivity. Opsin-based voltage reporters[7,8] contain retinal chromophores, which provides an opportunity to modify their absorption spectrum by regeneration with a retinal analogue. It has recently been shown that substitution of the native retinal chromophore with chemically synthesized analogues can induce up to a ∼200 nm red shift in the absorption maximum while maintaining the protein's ability to function as a proton pump or voltage indicator.[9−12] Together, these improvements can provide genetically encoded fluorescent voltage indicators that are compatible with optogenetic control, and with higher SNR and deeper tissue penetration capability to monitor membrane voltage changes with single-neuron sensitivity.

The ability to measure the absolute membrane voltage is important because it reflects various cellular processes where membrane potential is tightly regulated. Though the above-mentioned approaches allow for high-speed monitoring of neural activities by measuring relative membrane voltage changes, these measurements are based on fluorescence intensity changes, which are subject to many factors and

Received: May 10, 2019
Accepted: July 17, 2019
Published: July 17, 2019

DOI: 10.1021/acs.jpclett.9b01337
J. Phys. Chem. Lett. 2019, 10, 4374−4381

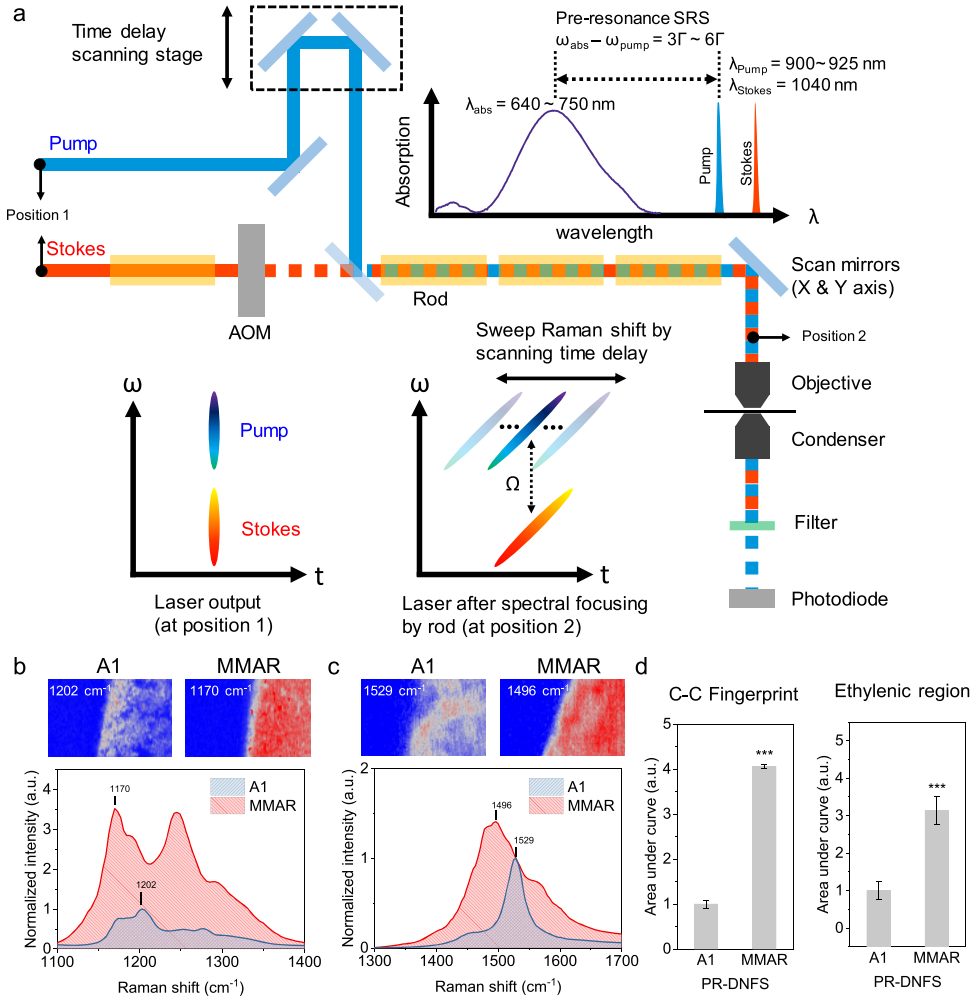

Figure 1. EPR-hSRS imaging of microbial rhodopsins in membrane fragments. (a) Schematic of the EPR-hSRS microscope. (b,c) SRS images and spectra of PR-DNFS-A1 and PR-DNFS-MMAR membrane fragments in (b) the C−C fingerprint region and (c) the ethylenic region. (d) Area under the curve from SRS spectra of PR-DNFS-A1 and PR-DNFS-MMAR in both spectral windows (n = 5). Error bars, SEM ***, p < 0.0001.

thus not suitable for absolute voltage measurement.[13] By ratiometric or fluorescence lifetime imaging of voltage indicators, absolute membrane voltage imaging was demonstrated in several studies.[14−16] By measuring the time-domain response of a rhodopsin-based voltage sensor, absolute membrane voltage imaging was reported,[17] but this required complex data analysis. Thus far, it remains challenging to convert fluorescence emission data into quantitative values representing the absolute voltage.[2,18]

Here, we present a new approach for potentially quantitative imaging of the membrane voltage by measuring the fingerprint vibrational signal of opsin-based voltage indicators under a stimulated Raman scattering (SRS) microscope. SRS microscopy is a quantitative imaging technique providing chemical bond information.[19,20] By recording a spectrum at each pixel, hyperspectral SRS microscopy further allows measurement of multiple species within a sample.[21−23] The Raman signals are sensitive to the environment of the molecules, and the spectral profile can be used as a signature of the membrane voltage.[24−26] SRS microscopy has a detection sensitivity down to the millimolar level.[27] Recent development of electronic preresonance SRS microscopy further increases the SNR by tuning the pump laser to the electronic preresonance region.[28,29] Using electronic preresonance hyperspectral SRS (EPR-hSRS) microscopy, we recorded the spectroscopic signatures of two red-shifted proteorhodopsin mutants containing a retinal analogue with one absorbing near 750 nm and a second absorbing near 630 nm.[9,12,30] We identified their voltage-sensitive peaks in the fingerprint regions similar to earlier spontaneous resonance Raman measurement of ARCH, the D95N archaeorhodopsin-3 mutant fluorescence voltage sensor,[31] and demonstrated the potential of using preresonance SRS imaging of NIR-absorbing microbial rhodopsins for quantitative mapping of the membrane voltage in single *E. coli* cells.

The proteorhodopsin mutants were expressed in *E. coli* and regenerated either with the native retinal (A1) or with the recently reported synthetic chromophore, 3-methylamino-16-nor-1,2,3,4-didehydroretinal (MMAR).[9] MMAR incorporation into a double mutant of proteorhodopsin PR-D212N-F234S yielding PR-DNFS-MMAR (Figure S1a) has been shown to dramatically shift the absorption maximum into the NIR region (>700 nm).[9,12] Smaller red shifts (80−100 nm) have been reported upon incorporation of MMAR in the single mutant PR-D97N[12,30] (termed PROPS-MMAR), which has been established as a voltage indicator in *E. coli*.[7] Our spectral data agree with the literature data (Figure S1b). The spectrum of PR-DNFS-MMAR showed an over 180 nm red shift in the

DOI: 10.1021/acs.jpclett.9b01337
J. Phys. Chem. Lett. 2019, 10, 4374−4381

absorption maximum relative to PR-DNFS-A1, which would be suitable for NIR excitation. The spectrum of PROPS-MMAR showed an ~80 nm red shift in the absorption maximum relative to PROPS-A1 (Figure S1b) and was strongly broadened and hence would allow NIR excitation of PROPS-MMAR for preresonance SRS.

Resonance Raman spectroscopic analysis has shown that the C−C fingerprint (1150 to 1300 cm^{-1}) and C═C ethylenic regions (1450−1600 cm^{-1}) provide information on molecular changes in microbial rhodopsins.[31−34] On the basis of Raman spectra of all-trans A1 and MMAR retinal (Figure S2), we identified several strong Raman peaks of these chromophores in the C−C fingerprint and C═C ethylenic regions that are distinctive from the Raman spectrum of *E. coli*. Note that the all-trans A1 Raman spectrum agrees with earlier Raman measurements.[35] Therefore, we targeted these two spectral windows for identifying the spectroscopic signatures of the MMAR-rhodopsins expressed in *E. coli* and to test for their dependence on the membrane potential. On the basis of previous studies employing electronic preresonance SRS imaging,[28,29] optimal enhancement of the SRS signal can be achieved with an attenuated electronic background when the pump beam (ω_{pump}) is tuned to a region away from the molecular absorption maximum (ω_{abs}) within $2\Gamma_e < \omega_{abs} - \omega_{pump} < 6\Gamma_e$, where Γ_e represents the homogeneous line width of the electronic transition of ~700 cm^{-1}.[28,29] For imaging in C−C fingerprint and ethylenic regions, the pump beam is set between 900 and 925 nm with a fixed 1040 nm Stokes beam. This pump beam range is within $3\Gamma_e-6\Gamma_e$ from the absorption of the NIR-absorbing microbial rhodopsins measured (λ = 633 to 751 nm), which is expected to generate electronic preresonance SRS signals with optimal signal-to-background ratio. Accordingly, we designed our EPR-hSRS microscope for imaging the NIR-absorbing microbial rhodopsins in *E. coli* with these specifications (Figure 1a and Experimental Methods).

The SRS spectra in the C−C fingerprint and ethylenic regions were recorded using 925 and 900 nm as pump wavelengths, respectively, with 1040 nm as the Stokes wavelength in both. To validate the SRS spectra of proteorhodopsins, we prepared PR-DNFS-MMAR reconstituted into *E. coli* polar lipids and performed EPR-hSRS imaging in both the C−C fingerprint and ethylenic spectral windows. These SRS spectra were in good agreement with resonance Raman spectra reported previously.[11,12] To further analyze the SRS spectra of PR-DNFS-MMAR, Lorentzian fitting was performed based on the peaks or shoulders identified in the Raman spectrum (Figure S3). The resulting cumulative fit reproduced the SRS spectra of PR-DNFS-MMAR with high fidelity (R^2 = 0.996 and 0.999 for C−C fingerprint and ethylenic regions, respectively). To validate that the SRS signal is enhanced through an electronic preresonance effect, we compared the SRS intensity of PR-DNFS-MMAR (λ_{abs} = 751 nm) with that of PR-DNFS-A1 (λ_{abs} = 563 nm). In the C−C fingerprint region, the peaks with the largest SRS cross section were found at 1202 cm^{-1} in PR-DNFS-A1 and at 1170 cm^{-1} in PR-DNFS-MMAR (Figure 1b). In the ethylenic region, the peak for the largest SRS cross section was also downshifted by ~33 cm^{-1} from 1529 cm^{-1} in PR-DNFS-A1 to 1496 cm^{-1} in PR-DNFS-MMAR (Figure 1c). Importantly, the SRS signals of these major peaks in NIR-absorbing PR-DNFS-MMAR were significantly higher than that of the non-NIR-absorbing PR-DNFS-A1 in both spectral windows (Figure 1d). We also note that the intensities of other SRS peaks in the same spectral window were enhanced. To quantify the signal enhancement by electronic preresonance effect, we obtained integration of the SRS signal in the whole spectral window. The integrated SRS signal from PR-DNFS-MMAR increased 4-fold in the C−C fingerprint region and increased 3-fold in the ethylenic region (Figure 1d) compared to PR-DNFS-A1. These data confirm that the SRS signal of the MMAR-chromophore is enhanced through an electronic preresonance effect and indicate that NIR-absorbing microbial rhodopsins are promising candidates for EPR-hSRS imaging.

For the voltage-sensing potential of microbial rhodopsins, a molecular mechanism has been proposed, involving a shift in the protonation equilibrium of the counterion/Schiff base complex, accompanying environmental changes such as in electric field strength.[8,31,36,37] It has been shown before that the Raman profile of MMAR chromophores is strongly pH dependent.[11,12] To test whether the SRS spectral profile recorded in *E. coli* can provide information on the protonation status of the counterion/Schiff base complex, we first exposed PR-DNFS-MMAR containing reconstituted membrane fragments to buffers with different pH values. Because the pK_a of the counterion (D97) in PR-DNFS-MMAR is ~8.0,[30,38] reconstituted PR-DNFS membranes at pH 7.0 mainly represent the protonated counterion, while at pH 9.5, a higher fraction of the counterion is deprotonated. In the C−C fingerprint window, the peak ratio of 1246 cm^{-1} to 1170 cm^{-1} was significantly reduced at pH 9.5 (Figure S4a,b). In contrast, the counterion in PROPS-MMAR is replaced by Asn (D97N) and the pK_a of the Schiff base is much higher (~9.6 [7]), and we did not observe significant spectral changes between pH 7 and 9.5 (Figure S5). Significantly, a similar effect was previously observed using stimulated Raman spectroscopy in PR-MMAR in detergent solution.[11] While the 1250 cm^{-1} band has not yet assigned, it has been suggested it arises from the aromatic C−N stretch that is specific to the MMAR chromophore.[11] One possible explanation for the effect of membrane potential on the peak ratio (I_{1246}/I_{1170}) is due to the response of the electronic structure of the MMAR chromophore to protonation of the counterion Asp97, which is facilitated by the presence of the methylamino group at the aromatic ring, which allows equivalent resonance structures in the MMAR chromophore.[11,30,39] This supports the concept that the spectral profile in the C−C fingerprint window is sensitive to the protonation state of the counterion/Schiff base complex of MMAR-rhodopsins.

To further test whether the ratio of the 1246 cm^{-1} to 1170 cm^{-1} peak can be used to map the membrane potential in *E. coli*, we performed EPR-hSRS imaging of *E. coli* expressing PR-DNFS-MMAR. *E. coli* in PBS buffer (pH 7.0) has been shown to maintain a negative membrane potential,[40] which would shift the counterion equilibrium toward the deprotonated state.[31] Indeed, PR-DNFS-MMAR in *E. coli* showed a 1246 cm^{-1} to 1170 cm^{-1} peak ratio, which is close to the one observed in the reconstituted membrane fragments at pH 9.5 (Figure S4c,d). Following collapse of the membrane potential of *E. coli* by gentle sonication, the 1246 cm^{-1} to 1170 cm^{-1} peak ratio increased significantly (Figure S4c,d). These results indicate that the 1246 cm^{-1} to 1170 cm^{-1} peak ratio can be used as a spectroscopic signature of the protonation state of the counterion/Schiff base complex in PR-DNFS-MMAR and that it responds to changes in membrane potential.

Compared to PR-DNFS, PROPS protein does not have light-induced proton pumping activity and would be a better

DOI: 10.1021/acs.jpclett.9b01337
J. Phys. Chem. Lett. 2019, 10, 4374−4381

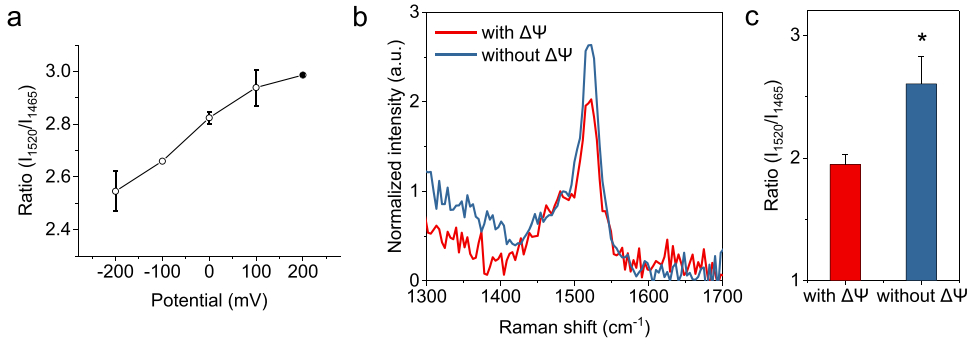

Figure 2. SRS spectroscopic signature of the membrane potential in PROPS-MMAR. (a) Plot of the ratio between I_{1520} and I_{1465} in PROPS-MMAR membrane fragments deposited on the ITO glass with different potentials applied across the membrane in PBS buffer (pH 7.0). All potentials were referred to the Ag/AgCl electrode. Mean ± standard deviation. (b) SRS spectra of PROPS-MMAR in *E. coli*. The membrane potential (ΔΨ) was eliminated by sonication. (c) Mean I_{1520}/I_{1465} of PROPS-MMAR in *E. coli* with intact ΔΨ (n = 3) and *E. coli* with disrupted ΔΨ (n = 3). Error bars, SEM. n.s., not significant. *, p < 0.05.

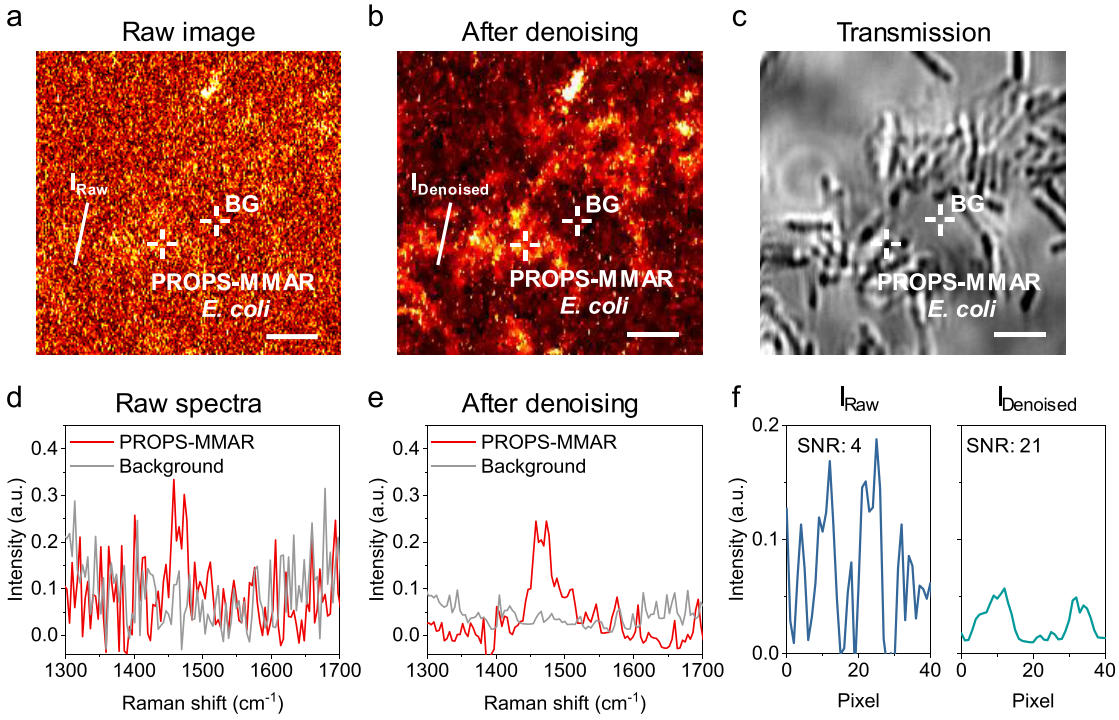

Figure 3. Denoising in spatial and spectral domains allows SRS imaging of single PROPS-MMAR-expressing *E. coli* cells. (a) Raw SRS image (1465 cm^{-1}) of PROPS-MMAR-expressing *E. coli* cells in PBS. (b) Denoised SRS image by the denoising algorithm. (c) Transmission image of the same field of view as that in (a). (d) Raw SRS spectra of a single PROPS-MMAR-expressing *E. coli* cell and background (BG) derived from four pixels as indicated in (a). (e) Denoised SRS spectra from the same positions. (f) Intensity cross section indicated with solid lines in (a) and (b). Scale bar: 5 μm.

voltage indicator. However, in agreement with the above result, we found that the C−C stretch fingerprint region of PROPS-MMAR when measured in *E. coli* is also insensitive to changes in membrane potential (Figure S6). We therefore investigated the SRS spectrum of PROPS in the ethylenic region. PROPS regenerated with native retinal (PROPS-A1) displays a peak at 1531 cm^{-1} (Figure S7a), which is in agreement with the previous Raman studies of PR and assigned to the C═C ethylenic stretch mode.[11,12] Compared to PROPS-A1, the $\nu_{C=C}$ of PROPS-MMAR was downshifted by 13 cm^{-1} to 1518 cm^{-1} (Figure S7b). Considering the red shift in λ_{max} between PROPS-MMAR and PROPS-A1 (78 nm), this downshift in frequency is in agreement with the empirical inverse relationship between λ_{max} and $\nu_{C=C}$.[12,41,42] A large downshift in frequency was also observed between PR-DNFS-A1 and PR-DNFS-MMAR (Figure 1c). Note, however, that fewer red-shifted species may also be present that are not resonance-enhanced by the SRS measurements but do appear using 532 nm probe excitation.[12]

To evaluate if the SRS spectral profile in the ethylenic window can serve as a quantitative signature for the membrane potential, we deposited a reconstituted PROPS-MMAR membrane on the indium tin oxide (ITO)-coated glass slide to form multilamellar films and applied voltage by a potentiostat across the deposited membrane fragments while they were immersed in PBS buffer. After spectral analysis of the EPR-hSRS images of the membrane fragments at different potentials, we found linear correlation between the 1520 cm^{-1}

DOI: 10.1021/acs.jpclett.9b01337
J. Phys. Chem. Lett. 2019, 10, 4374−4381

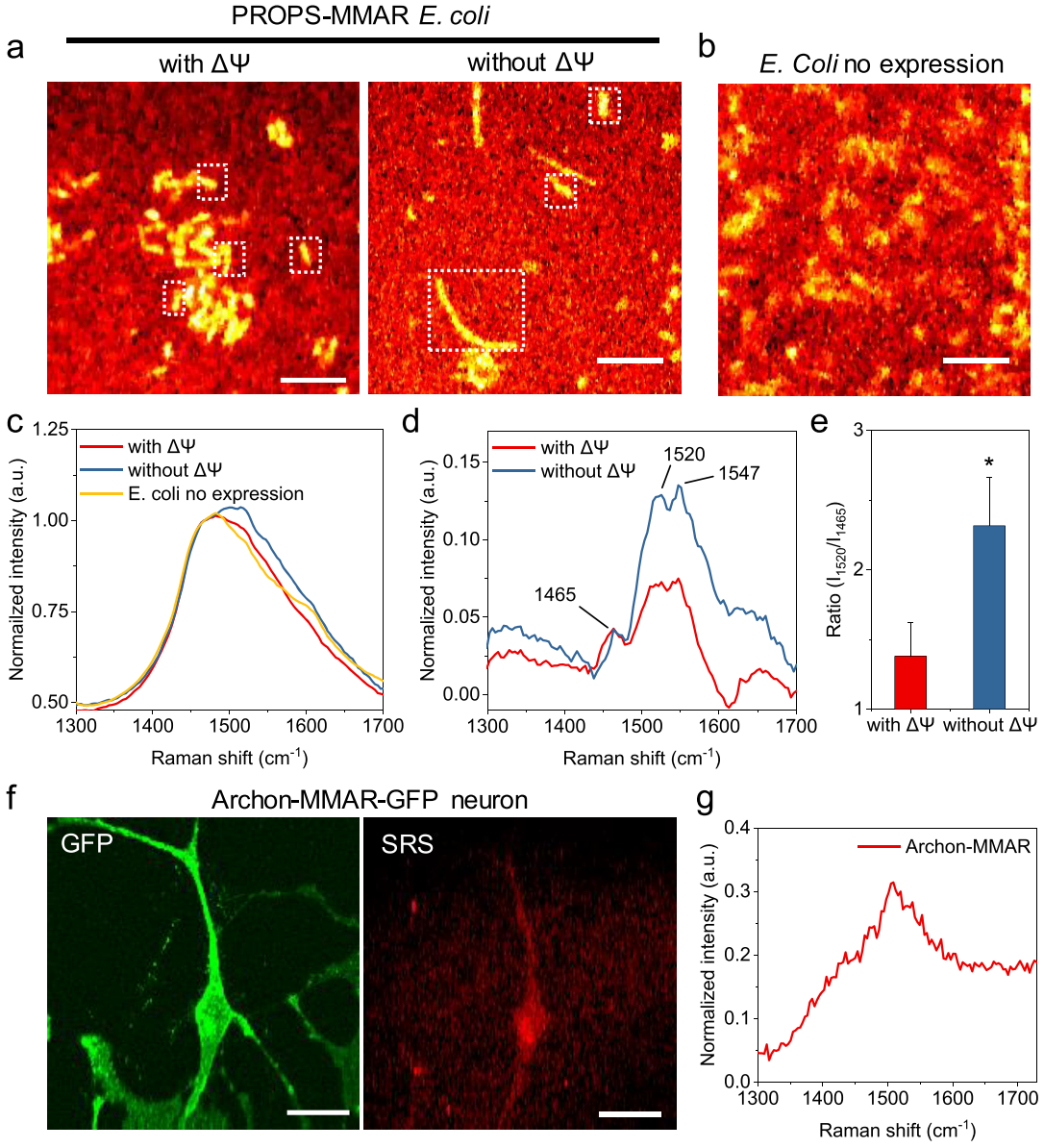

Figure 4. EPR-hSRS imaging of PROPS-MMAR in single *E. coli* cells for sensing the membrane potential. (a) SRS images (1465 cm^{-1}) of PROPS-MMAR-expressing *E. coli* cells in PBS. The membrane potential ($\Delta\Psi$) was eliminated by sonication. The images were subjected to a denoising algorithm. (b) SRS image of *E. coli* cells with no PROPS-MMAR expression in PBS. Scale bar: 5 μm. (c) Representative raw SRS spectra from single *E. coli* cells. (d) SRS spectra of PROPS-MMAR *E. coli* with different $\Delta\Psi$ values after subtraction of the *E. coli* background. (e) Statistical analysis of spectral differences between PROPS-MMAR *E. coli* with $\Delta\Psi$ ($n = 4$) and without $\Delta\Psi$ ($n = 3$). Error bars, SEM. *, $p < 0.05$. (f) Two-photon fluorescence and SRS images (1508 cm^{-1}) of Archon-MMAR-GFP-expressing rat cortical neurons at resting potential. GFP signal is used to confirm the expression of Archon protein. Scale bar: 10 μm. (g) SRS spectra of Archon-MMAR from a single neuron at resting potential after subtraction of the neuron background.

to 1465 cm^{-1} peak ratio and potential applied from −250 to +250 mV (Figure 2a). Using this spectroscopic signature, we performed EPR-hSRS imaging of *E. coli* expressing PROPS-MMAR. When the membrane potential of the *E. coli* was disrupted by sonication, the 1520 cm^{-1} to 1465 cm^{-1} peak ratio increased significantly (Figure 2b,c). These results suggest that the SRS spectral profile of PROPS-MMAR in the ethylenic window can be used for membrane potential imaging in *E. coli*.

To validate EPR-hSRS voltage imaging in single cells, PROPS-MMAR-expressing *E. coli* cells were immobilized on poly-L-lysine-coated coverslips and imaged using EPR-hSRS in the ethylenic region (Figure 3). As expected, a relatively weak SRS signal was obtained from single *E. coli* cells due to the lower concentration and volume of PROPS-MMAR probed compared to the bulk measurement of PROPS-MMAR-expressing *E. coli* in a capillary (Figure 3a). By applying a denoising algorithm based on total variation minimization[43] (Figure 3b), the spectral resolution improved significantly (Figure 3d,e). At the same time, the denoising algorithm improved the SNR in the spatial domain about 5-fold (Figure 3f), allowing differentiation of single *E. coli* cells. This significant improvement in SNR enabled visualization of SRS spectra from single PROPS-MMAR-expressing *E. coli* cells (Videos S1 and S2).

DOI: 10.1021/acs.jpclett.9b01337
J. Phys. Chem. Lett. 2019, 10, 4374−4381

To verify voltage imaging using the C═C signature of PROPS-MMAR in single *E. coli* cells, we performed EPR-hSRS imaging of PROPS-MMAR-expressing *E. coli* cells with an intact unsonicated or collapsed transmembrane potential after sonication (Figure 4a). The SRS spectra from single PROPS-MMAR-expressing *E. coli* cells displayed a prominent peak at 1480 cm^{-1} with weak shoulders at higher wavenumber (Figure 4c). We note that this spectral profile from single *E. coli* cells differs considerably from that of reconstituted membrane fragments (Figure S7). This is likely due to the high endogenous background signal from *E. coli*. Indeed, the SRS spectrum from an *E. coli* cell without PROPS-MMAR expression also showed a strong peak at 1480 cm^{-1} (Figure 4b,c). Hence, not surprisingly, the SRS spectra of a PROPS-MMAR-expressing *E. coli* cell are a superposition of the signal from PROPS-MMAR and the background from *E. coli*. To extract the PROPS-MMAR signal, the SRS spectrum of PROPS-free *E. coli* was subtracted from the SRS spectra of PROPS-MMAR-expressing *E. coli*. After noise and background removal, a distinct spectral profile of PROPS-MMAR was obtained from single *E. coli* (Figure 4d), which is quite similar to bulk measurement of *E. coli* expressing PROPS-MMAR in a capillary (Figure 2b). We note that the appearance of a peak at 1547 cm^{-1} in the single *E. coli* cells after background removal, which might be the contribution of the amide II band (1520−1570 cm^{-1}) from the cytoplasm of *E. coli* cells. Consistent with the bulk measurement of PROPS-MMAR-expressing *E. coli* in a capillary, the 1520 cm^{-1} to 1465 cm^{-1} peak ratio significantly increased when the membrane potential was disrupted in *E. coli* cells compared to the peak ratio in depolarized (i.e., normal negative membrane potential) *E. coli* cells (Figure 4d). Statistical analysis of multiple cells demonstrated multicell voltage imaging and corroborated our observation that the SRS peak at ∼1520 cm^{-1} is voltage-sensitive (Figure 4e). These results collectively indicate that the 1520 cm^{-1} to 1465 cm^{-1} peak ratio can be used as a spectroscopic signature of the membrane potential and EPR-SRS imaging allows membrane potential detection with single *E. coli* cell sensitivity. To show the potential of applying EPR-hSRS to map the membrane voltage in neurons, we pursued two-photon fluorescence and SRS imaging of an MMAR-incorporated voltage sensor, Archons,[5] expressed in rat cortical neurons (Figure 4f). In the fingerprint region, a similar peak at around 1508 cm^{-1} is clearly identified as the SRS signal from Archon-MMAR (Figure 4g).

While the voltage and pH-induced changes that we observe in the C═C stretch ethylenic region are not yet understood on a molecular level, they may reflect changes in the charge distribution and resonance state of the chromophore. In fact, in an earlier study using NIR resonance Raman confocal microscopy, *E. coli* expressing the D95N mutant of AR3, which is homologous to PROPS (the mutant D97N of PR), was observed to cause changes in both the fingerprint and ethylenic regions due to alterations in the membrane potential.[31] These changes were attributed to the effects of the membrane potential on the protonation state of the Schiff base of an N-like species that exists even in the unphotolyzed state in equilibrium with an O-like species.

This study demonstrates the feasibility of the novel concept of performing quantitative voltage imaging by measuring the voltage-sensitive spectral signatures of membrane potential reporters using EPR-hSRS. An electronic preresonance configuration significantly enhanced the SRS signal, allowing hyperspectral SRS imaging of voltage indicators with sufficient sensitivity to probe single *E. coli* cells. Importantly, the use of light with wavelengths > 700 nm to obtain EPR-hSRS opens the possibility of voltage imaging of deep tissues that strongly absorb and scatter visible light.[6] For example, EPR-hSRS imaging of bacterial pathogens in intact tissues, even in living animals, can reveal information about the state of these pathogens and even the mechanism of pathogenesis. While proteorhodopsin does not express well in animal cells, a similar application of EPR-hSRS imaging to other MMAR-containing microbial rhodopsins such as Archaerhodopsin-3 (AR3)[39] and AR3-derived voltage sensors known as QuasArs[44] and Archons[5] that do express well in animal cells is also feasible (Figure 4f,g). One of the important considerations is the imaging speed. Our current work demonstrates imaging of the resting membrane potential change with a 10 μs pixel dwell time, which takes 120−360 ms to image an SRS spectrum of a single *E. coli* (100−300 pixels, 120 frames for hyperspectral SRS stack). This imaging speed is sufficient to monitor spiking in *E. coli* cells (one spike lasts for 1−40 s[7]) but not fast enough for action potentials in neurons. The recent advances in hyperspectral SRS imaging setup, such as the multiplex SRS system (32 μs pixel dwell time for an SRS spectrum)[45] and polygonal scanning-based SRS system (0.1 μs pixel dwell time for an SRS spectrum),[46] provide promising approaches. In summary, we identified two potential SRS spectral profile windows for quantitative imaging of the membrane potential in proteorhodopsins containing the red-shifting analogue chromophore MMAR. SRS imaging in combination with such NIR-sensitive microbial rhodopsin voltage sensors provides novel prospects for mapping the absolute membrane potential in living cells, from bacteria up to neurons.

■ ASSOCIATED CONTENT

Supporting Information

The Supporting Information is available free of charge on the ACS Publications website at DOI: 10.1021/acs.jpclett.9b01337.

Experimental methods and figures showing generation of NIR-absorbing microbial rhodopsins, Raman spectra of A1 and MMAR, EPR-hSRS spectra, SRS spectroscopic signatures, and the SRS spectral profile in the C−C fingerprint region (PDF)

Hyperspectral SRS movie of single PROPS-MMAR-expressing *E. coli* cells (AVI)

Hyperspectral SRS movie of single PROPS-MMAR-expressing *E. coli* cells (AVI)

■ AUTHOR INFORMATION

Corresponding Authors

*E-mail: jxcheng@bu.edu (J.-X.C.).
*E-mail: kjr@bu.edu (K.J.R.).

ORCID

Hyeon Jeong Lee: 0000-0002-2417-9338
Kai-Chih Huang: 0000-0002-3419-825X
Willem J. DeGrip: 0000-0001-7637-4920
Kenneth J. Rothschild: 0000-0002-2847-6671
Ji-Xin Cheng: 0000-0002-5607-6683

Notes

The authors declare no competing financial interest.

DOI: 10.1021/acs.jpclett.9b01337
J. Phys. Chem. Lett. 2019, 10, 4374−4381

■ ACKNOWLEDGMENTS

This work was partially supported by a Science & Engineering Keck Grant to J.X.C. and a grant from the National Science Foundation Division of Chemical, Bioengineering, Environmental and Transport Systems (CBET-1264434) to K.J.R. W.D.J. was supported by the research program of BioSolar Cells (BSC Core Project Grant C2.9), co-financed by the Dutch Ministry of Economic Affairs. The authors thank Joel Kralj for helpful discussion and for providing the pBAD D97N (PROPS) plasmid for expression of GPR-D97N in *E. coli*. The authors thank Kiryl D. Piatkevich and Edward S. Boyden for providing the Archon virus for expression in neurons and thank Hengye Man for providing neuron cultures.

■ REFERENCES

(1) Lin, M. Z.; Schnitzer, M. J. Genetically encoded indicators of neuronal activity. *Nat. Neurosci.* **2016**, *19*, 1142−1153.
(2) Xu, Y.; Zou, P.; Cohen, A. E. Voltage imaging with genetically encoded indicators. *Curr. Opin. Chem. Biol.* **2017**, *39*, 1−10.
(3) Ordaz, J. D.; Wu, W.; Xu, X. M. *Neural Regener. Res.* **2017**, *12*, 1197−1209.
(4) St-Pierre, F.; Chavarha, M.; Lin, M. Z. Designs and sensing mechanisms of genetically encoded fluorescent voltage indicators. *Curr. Opin. Chem. Biol.* **2015**, *27*, 31−38.
(5) Piatkevich, K. D.; Jung, E. E.; Straub, C.; Linghu, C.; Park, D.; Suk, H. J.; Hochbaum, D. R.; Goodwin, D.; Pnevmatikakis, E.; Pak, N.; et al. A robotic multidimensional directed evolution approach applied to fluorescent voltage reporters. *Nat. Chem. Biol.* **2018**, *14*, 352−360.
(6) Chernov, K. G.; Redchuk, T. A.; Omelina, E. S.; Verkhusha, V. V. Near-Infrared Fluorescent Proteins, Biosensors, and Optogenetic Tools Engineered from Phytochromes. *Chem. Rev.* **2017**, *117*, 6423−6446.
(7) Kralj, J. M.; Hochbaum, D. R.; Douglass, A. D.; Cohen, A. E. Electrical spiking in Escherichia coli probed with a fluorescent voltage-indicating protein. *Science* **2011**, *333*, 345−348.
(8) Kralj, J. M.; Douglass, A. D.; Hochbaum, D. R.; Maclaurin, D.; Cohen, A. E. Optical recording of action potentials in mammalian neurons using a microbial rhodopsin. *Nat. Methods* **2012**, *9*, 90−95.
(9) Ganapathy, S.; Venselaar, H.; Chen, Q.; de Groot, H. J.; Hellingwerf, K. J.; de Grip, W. J. Retinal-Based Proton Pumping in the Near Infrared. *J. Am. Chem. Soc.* **2017**, *139*, 2338−2344.
(10) Herwig, L.; Rice, A. J.; Bedbrook, C. N.; Zhang, R. K.; Lignell, A.; Cahn, J. K. B.; Renata, H.; Dodani, S. C.; Cho, I.; Cai, L.; et al. Directed Evolution of a Bright Near-Infrared Fluorescent Rhodopsin Using a Synthetic Chromophore. *Cell Chem. Biol.* **2017**, *24*, 415−425.
(11) Hontani, Y.; Ganapathy, S.; Frehan, S.; Kloz, M.; de Grip, W. J.; Kennis, J. T. M. Strong pH-Dependent Near-Infrared Fluorescence in a Microbial Rhodopsin Reconstituted with a Red-Shifting Retinal Analogue. *J. Phys. Chem. Lett.* **2018**, *9*, 6469−6474.
(12) Mei, G.; Mamaeva, N.; Ganapathy, S.; Wang, P.; de Grip, W. J.; Rothschild, K. J. Raman spectroscopy of a near infrared absorbing proteorhodopsin: Similarities to the bacteriorhodopsin O photointermediate. *PLoS One* **2018**, *13*, No. e0209506.
(13) Vogt, N. Voltage sensors: challenging, but with potential. *Nat. Methods* **2015**, *12*, 921−924.
(14) Gross, E.; Bedlack, R. S.; Loew, L. M. Dual-wavelength ratiometric fluorescence measurement of the membrane dipole potential. *Biophys. J.* **1994**, *67*, 208−216.
(15) Zhang, J.; Davidson, R. M.; Wei, M. D.; Loew, L. M. Membrane electric properties by combined patch clamp and fluorescence ratio imaging in single neurons. *Biophys. J.* **1998**, *74*, 48−53.
(16) Brinks, D.; Klein, A.; Cohen, A. Two-Photon Lifetime Imaging of Voltage Indicating Proteins as a Probe of Absolute Membrane Voltage. *Biophys. J.* **2015**, *109*, 914−921.
(17) Hou, J. H.; Venkatachalam, V.; Cohen, A. E. Temporal dynamics of microbial rhodopsin fluorescence reports absolute membrane voltage. *Biophys. J.* **2014**, *106*, 639−648.
(18) Yang, H. H.; St-Pierre, F. Genetically Encoded Voltage Indicators: Opportunities and Challenges. *J. Neurosci.* **2016**, *36*, 9977−9989.
(19) Freudiger, C. W.; Min, W.; Saar, B. G.; Lu, S.; Holtom, G. R.; He, C.; Tsai, J. C.; Kang, J. X.; Xie, X. S. Label-free biomedical imaging with high sensitivity by stimulated Raman scattering microscopy. *Science* **2008**, *322*, 1857−1861.
(20) Cheng, J. X.; Xie, X. S. Vibrational spectroscopic imaging of living systems: An emerging platform for biology and medicine. *Science* **2015**, *350*, aaa8870.
(21) Fu, D.; Holtom, G.; Freudiger, C.; Zhang, X.; Xie, X. S. Hyperspectral imaging with stimulated Raman scattering by chirped femtosecond lasers. *J. Phys. Chem. B* **2013**, *117*, 4634−4640.
(22) Wang, P.; Li, J.; Wang, P.; Hu, C.-R.; Zhang, D.; Sturek, M.; Cheng, J.-X. Label-free quantitative imaging of cholesterol in intact tissues by hyperspectral stimulated Raman scattering microscopy. *Angew. Chem., Int. Ed.* **2013**, *52*, 13042−13046.
(23) Zhang, D.; Wang, P.; Slipchenko, M. N.; Ben-Amotz, D.; Weiner, A. M.; Cheng, J. X. Quantitative vibrational imaging by hyperspectral stimulated Raman scattering microscopy and multivariate curve resolution analysis. *Anal. Chem.* **2013**, *85*, 98−106.
(24) Mikkelsen, R. B.; Verma, S. P.; Wallach, D. F. Effect of transmembrane ion gradients on Raman spectra of sealed, hemoglobin-free erythrocyte membrane vesicles. *Proc. Natl. Acad. Sci. U. S. A.* **1978**, *75*, 5478−5482.
(25) Liu, B.; Lee, H. J.; Zhang, D.; Liao, C.-S.; Ji, N.; Xia, Y.; Cheng, J.-X. Label-free spectroscopic detection of membrane potential using stimulated Raman scattering. *Appl. Phys. Lett.* **2015**, *106*, 173704.
(26) Lee, H. J.; Zhang, D.; Jiang, Y.; Wu, X.; Shih, P. Y.; Liao, C. S.; Bungart, B.; Xu, X. M.; Drenan, R.; Bartlett, E.; et al. Label-Free Vibrational Spectroscopic Imaging of Neuronal Membrane Potential. *J. Phys. Chem. Lett.* **2017**, *8*, 1932−1936.
(27) Zhang, D.; Slipchenko, M. N.; Cheng, J.-X. Highly sensitive vibrational imaging by femtosecond pulse stimulated Raman loss. *J. Phys. Chem. Lett.* **2011**, *2*, 1248−1253.
(28) Wei, L.; Chen, Z.; Shi, L.; Long, R.; Anzalone, A. V.; Zhang, L.; Hu, F.; Yuste, R.; Cornish, V. W.; Min, W. Super-multiplex vibrational imaging. *Nature* **2017**, *544*, 465−470.
(29) Wei, L.; Min, W. Electronic Preresonance Stimulated Raman Scattering Microscopy. *J. Phys. Chem. Lett.* **2018**, *9*, 4294−4301.
(30) Ganapathy, S. *Improvisations in Phototrophy, Protein engineering and functional investigation of rhodopsin proton-pumps*; Ph.D. Thesis, Leiden University, 2017.
(31) Saint Clair, E. C.; Ogren, J. I.; Mamaev, S.; Russano, D.; Kralj, J. M.; Rothschild, K. J. Near-IR resonance Raman spectroscopy of archaerhodopsin 3: effects of transmembrane potential. *J. Phys. Chem. B* **2012**, *116*, 14592−14601.
(32) Braiman, M.; Mathies, R. Resonance Raman spectra of bacteriorhodopsin's primary photoproduct: evidence for a distorted 13-cis retinal chromophore. *Proc. Natl. Acad. Sci. U. S. A.* **1982**, *79*, 403−407.
(33) Argade, P. V.; Rothschild, K. J. Quantitative analysis of resonance Raman spectra of purple membrane from Halobacterium halobium: L550 intermediate. *Biochemistry* **1983**, *22*, 3460−3466.
(34) Smith, S. O.; Braiman, M. S.; Myers, A. B.; Pardoen, J. A.; Courtin, J. M. L.; Winkel, C.; Lugtenburg, J.; Mathies, R. A. Vibrational analysis of the all-trans-retinal chromophore in light-adapted bacteriorhodopsin. *J. Am. Chem. Soc.* **1987**, *109*, 3108−3125.
(35) Curry, B.; Broek, A.; Lugtenburg, J.; Mathies, R. Vibrational analysis of all-trans-retinal. *J. Am. Chem. Soc.* **1982**, *104*, 5274−5286.
(36) Kolodner, P.; Lukashev, E. P.; Ching, Y. C.; Rousseau, D. L. Electric-field-induced Schiff-base deprotonation in D85N mutant bacteriorhodopsin. *Proc. Natl. Acad. Sci. U. S. A.* **1996**, *93*, 11618−11621.

DOI: 10.1021/acs.jpclett.9b01337
J. Phys. Chem. Lett. 2019, 10, 4374−4381

(37) Maclaurin, D.; Venkatachalam, V.; Lee, H.; Cohen, A. E. Mechanism of voltage-sensitive fluorescence in a microbial rhodopsin. *Proc. Natl. Acad. Sci. U. S. A.* **2013**, *110*, 5939−5944.
(38) Kim, S. Y.; Waschuk, S. A.; Brown, L. S.; Jung, K. H. Screening and characterization of proteorhodopsin color-tuning mutations in Escherichia coli with endogenous retinal synthesis. *Biochim. Biophys. Acta, Bioenerg.* **2008**, *1777*, 504−513.
(39) Ganapathy, S.; Kratz, S.; Chen, Q.; Hellingwerf, K. J.; de Groot, H. J. M.; Rothschild, K. J.; de Grip, W. J. Red Shifted and Near-infrared Active Analog Pigments Based upon Archaerhodopsin-3. *Photochem. Photobiol.* **2019**, DOI: 10.1111/php.13093.
(40) Zilberstein, D.; Agmon, V.; Schuldiner, S.; Padan, E. Escherichia coli intracellular pH, membrane potential, and cell growth. *J. Bacteriol.* **1984**, *158*, 246−252.
(41) Aton, B.; Doukas, A. G.; Callender, R. H.; Becher, B.; Ebrey, T. G. Resonance Raman studies of the purple membrane. *Biochemistry* **1977**, *16*, 2995−2999.
(42) Ogren, J. I.; Mamaev, S.; Russano, D.; Li, H.; Spudich, J. L.; Rothschild, K. J. Retinal chromophore structure and Schiff base interactions in red-shifted channelrhodopsin-1 from Chlamydomonas augustae. *Biochemistry* **2014**, *53*, 3961−3970.
(43) Liao, C. S.; Choi, J. H.; Zhang, D.; Chan, S. H.; Cheng, J. X. Denoising Stimulated Raman Spectroscopic Images by Total Variation Minimization. *J. Phys. Chem. C* **2015**, *119*, 19397−19403.
(44) Hochbaum, D. R.; Zhao, Y.; Farhi, S. L.; Klapoetke, N.; Werley, C. A.; Kapoor, V.; Zou, P.; Kralj, J. M.; Maclaurin, D.; Smedemark-Margulies, N.; et al. All-optical electrophysiology in mammalian neurons using engineered microbial rhodopsins. *Nat. Methods* **2014**, *11*, 825−833.
(45) Liao, C.-S.; Slipchenko, M. N.; Wang, P.; Li, J.; Lee, S.-Y.; Oglesbee, R. A.; Cheng, J.-X. Microsecond scale vibrational spectroscopic imaging by multiplex stimulated Raman scattering microscopy. *Light: Sci. Appl.* **2015**, *4*, No. e265.
(46) Lin, H.; Deng, F.; Huang, K.-C.; Lee, H. J.; Cheng, J.-X. *CLEO: Applications and Technology*; Optical Society of America, 2019; p ATu3K.3.

DOI: 10.1021/acs.jpclett.9b01337
J. Phys. Chem. Lett. 2019, 10, 4374−4381